Title

Structure and Thermodynamics of Homogeneous-Dendritic-Polymer Solutions: Computer Simulation, Integral Equation, and Lattice-Cluster Theory

Journal

Macromolecules, 30(21)

Author

Lue, Leo

Publication Date

1997

LBNL-39960
UC-401

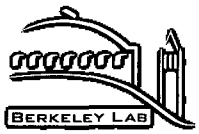

ERNEST ORLANDO LAWRENCE
BERKELEY NATIONAL LABORATORY

Structure and Thermodynamics of Homogeneous-Dendritic-Polymer Solutions: Computer Simulation, Integral Equation, and Lattice-Cluster Theory

Leo Lue and John M. Prausnitz
Chemical Sciences Division

January 1997
Submitted to
Polymer Science and Engineering

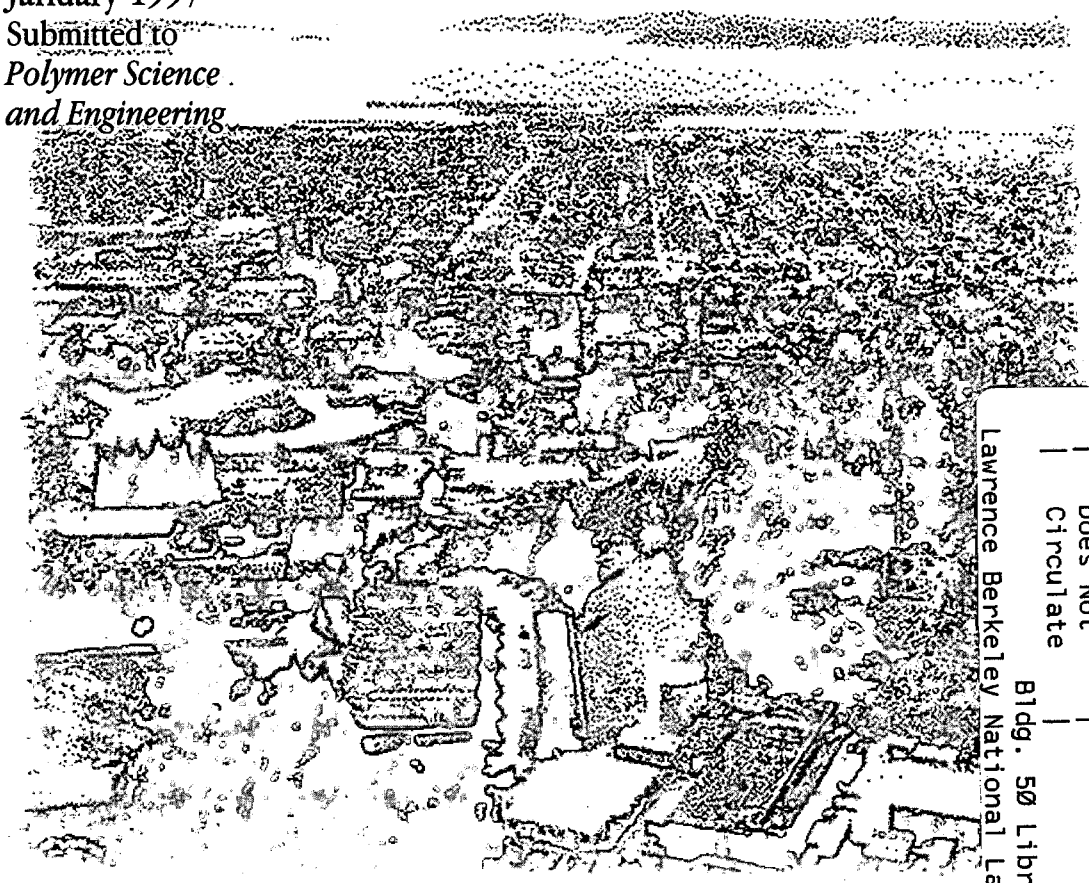

LBNL-39960

DISCLAIMER

LBNL-39960
UC-401

Structure and Thermodynamics of Homogeneous-Dendritic-Polymer Solutions: Computer Simulation, Integral Equation, and Lattice-Cluster Theory

Leo Lue and John M. Prausnitz*

Department of Chemical Engineering

University of California, Berkeley

and

Chemical Sciences Division

Lawrence Berkeley National Laboratory

Berkeley, CA 94720, USA

This work was supported by the Director, Office of Energy Research, Office of Basic Energy Sciences, Chemical Sciences Division of the U.S. Department of Energy under Contract Number DE-AC03-76SF00098.

*Author to whom correspondence should be addressed.

STRUCTURE AND THERMODYNAMICS OF HOMOGENEOUS-DENDRITIC-POLYMER SOLUTIONS: COMPUTER SIMULATION, INTEGRAL EQUATION, AND LATTICE-CLUSTER THEORY

Leo Lue and John M. Prausnitz*
Department of Chemical Engineering
University of California, Berkeley
and
Chemical Sciences Division
Lawrence Berkeley National Laboratory
Berkeley, CA 94720

We present some calculated structural and thermodynamic properties of homogeneous-dendritic-polymer solutions using computer-simulation methods, integral-equation theory, and lattice-cluster theory.

Monte-Carlo methods are used to sample conformations of polymer molecules. From these conformations, we first compute two properties of the polymer: the distribution of segments within the molecule and the radius of gyration. Simulations for non-attracting polymer pairs give the potential of mean force and the second virial coefficient. Given the potential of mean force between polymer molecules, we use integral-equation theory to calculate the equation of state of an athermal solution at low polymer concentrations.

We apply lattice-cluster theory to obtain solvent activities and liquid-liquid equilibria for homogeneous-dendritic polymers in a non-athermal concentrated solution. There is little difference between the vapor pressures of solutions of linear polymers and homogeneous-dendritic polymers. However, there is a modest difference between the liquid-liquid coexistence curve for linear-polymer solutions and homogeneous-dendrimer solutions. The critical temperatures of dendrimer solutions are lower than those of solutions containing corresponding linear polymers. This difference rises with increasing generation number and decreasing separator length.

*Author to whom correspondence should be addressed.

I. INTRODUCTION

In recent years, chemists have been able to synthesize highly symmetric, hyperbranched macromolecules known as dendrimers.[1] Possible applications[2] of dendrimers include nanoscale catalysts,[3] nanoscale reaction vessels, micelle mimics,[4–6] magnetic resonance imaging agents,[7] immunodiagnostics, agents for delivering drugs or genes into cells, chemical sensors, information-processing materials, high-performance polymers, adhesives and coatings, separation media, and molecular antennae for absorbing light. Despite the wealth of possible applications, little work has been reported on the thermodynamic properties of solutions containing dendritic polymers. Here we present some results for solutions of homogeneous-dendritic polymers obtained from molecular simulation, integral-equation theory, and lattice-cluster theory.

Most previous theoretical work for dendritic polymers has focused on determining the structure of isolated homogeneous dendrimers. One of the first attempts at modeling dendritic polymers was by de Gennes and Hervet, who developed a self-consistent mean-field theory for the distribution of polymer segments within the dendrimer molecule.[8] Biswas and Cherayil have performed[9] renormalization-group calculations to determine how the average center-to-end distance of a dendrimer depends on its generation number and separator length. However, both of these theories assume that the separator is extremely flexible; that assumption is not valid for the dendrimers that are now produced by synthetic chemists.

In addition to these analytical studies, Boris and Rubinstein have performed[10] numerical self-consistent mean-field calculations for individual dendrimers.

Computer simulations have been performed to determine the structure of isolated homogeneous dendritic polymers. Lescanec and Muthukumar have reported[11] off-lattice simulations for dendrimers composed of tangent hard spheres; they obtained the density distribution of segments within the dendrimer, as well as the scaling of the radius of gyration with the molecular weight and spacer length of the dendrimer, but these simulations were for "randomly" grown dendrimers, and thus do not represent the structure of dendrimer molecules in solution. Naylor and coworkers have reported[12] Monte-Carlo simulations of sophisticated molecular models of dendritic polymers. Mansfield and Klushin performed[13] Monte-Carlo simulations for dendritic polymers on a diamond lattice and obtained various single-polymer structural properties. Murat and Grest performed[14] molecular-dynamics simulations for isolated dendrimers in solvents of varying qualities. Chen and Cui have performed[15] Monte-Carlo simulations for athermal hard sphere dendrimers.

Lattice theories, in particular the mean-field theories of Flory-Huggins[16] and Guggenheim,[17] have contributed much to our understanding of polymer solutions. However, most of these lattice theories fail to yield any dependence of solution properties on polymer architecture. In recent years, Freed and coworkers have developed a systematic expansion of the partition function of lattice polymers, known as lattice-cluster theory (LCT).[18,19] This theory takes into account the effect of branching on the thermodynamic properties of concentrated polymer solutions.

In this work we study the effect of polymer structure on the thermodynamic properties of homogeneous-dendritic-polymer solutions using Monte-Carlo simulations and integral-

equation theory, at low polymer concentrations; for intermediate and high polymer concentrations, we apply LCT.

Section II describes our Monte-Carlo simulations for non-attracting dendritic polymers. For the isolated polymer, we compute the distribution of segments about the polymer center of mass and the polymer radius of gyration. We then report the potential of mean force for several non-attracting dendrimers and compare them to those of linear chains of the same molecular weight. In addition, we calculate second virial coefficients for dendrimers of various generations and separator lengths. Also in this section, we apply integral-equation theory to obtain the variation of pressure with polymer concentration. In Section III, we report our calculations for dendrimers using non-athermal lattice-cluster theory. First we present the formulae required for applying this theory to dendritic polymers. Then we present results for the vapor pressures of binary polymer-solvent solutions and their liquid-liquid coexistence curves. Finally in Section IV, we summarize and discuss our results.

II. DILUTE POLYMER SOLUTIONS

Description of Model

The polymer molecule is constructed by tangent hard spheres as shown in Figure 1. The linear chain is characterized by the total number of sites, M. The dendrimer is characterized by two parameters: the generation number, g, and the separator length, n. It possesses a central core site which is attached to three arms. Each of these arms branches into two additional arms; both of these branch into two arms. The generation number, g, is the number of times this branching process occurs. The separator length, n, is the number of bonds in each arm between branch points. At each branch site, the angle between sites is fixed at 120°.

Polymer Structure at Infinite Dilution

We begin with Monte Carlo simulations of an isolated polymer molecule. We sample various polymer conformations with the pivot algorithm.[20] Beginning with an initial polymer configuration, a segment on the molecule is randomly chosen. We bend the molecule at the chosen segment by a random angle. If the new configuration generated by this process is allowed, that is, if it does not posess any overlapping spheres, then the configuration is accepted. Otherwise, the new configuration is discarded, and the initial configuration is retained. For each conformation, the property of interest (e.g., the radius of gyration) is computed, and its value is added to a running average.

For each dendrimer, five separate runs were performed, each consisting of 10^6 conformations. Reported properties are the averages of these five runs.

These simulations yield structural properties of the polymer: the distribution of segments within the polymer and its mean radius of gyration, as a function of the chemical structure of the polymer and its molecular weight.

Figure 2 shows the density distribution of sites about the center of mass for a linear polymer with 91 segments (solid line) and a third-generation dendrimer with $n = 2$ (dashed line). The dendritic polymer has a more compact distribution of segments than the linear polymer, and the density of segments is much higher near its center of mass. The dendrimer exhibits a slight shoulder at about $r = R_g$, a result of the hyperbranched nature of the dendrimer.

Figure 3 shows the segment-density distribution about the center of mass for second-generation dendrimers with $n = 2$ (solid line), $n = 5$ (dashed line), and $n = 10$ (dotted line). The shoulder at $r = R_g$ becomes more pronounced and the density of sites near the dendrimer center of mass increases as the spacer length, n, decreases. Unlike the predictions of Hervet and de Gennes,[8] the dendrimers do not possess a hollow core, in agreement with the simulations of Mansfield and Klushin.[13–15]

In Figure 4, we plot the distribution of sites for several dendrimers with $n = 2$. The solid line is for a generation-two dendrimer; the dashed line is for a generation-three dendrimer; the dotted line is for a generation-four dendrimer; and the dashed-dotted line is for a generation-five dendrimer. The shoulder at $r = R_g$ becomes more pronounced with increasing generation number and becomes a secondary peak at a high enough generation number. To perform simulations for dendrimers of generation six or higher, we need to employ a more sophisticated Monte-Carlo method, such as the extended continuum-configuration-bias method;[21] such simulations are not reported here.

The self-consistent mean-field predictions of Boris and Rubinstein[10] for the segment density profiles of dendrimers of various generations do not possess a secondary peak or a shoulder, in disagreement with simulation results.[13–15] This disagreement indicates that a mean-field theory is not applicable because it does not properly account for strong long-range correlations between segments on the dendrimer due to bonding constraints. It appears that the mean-field approximation may not capture even the qualitative structural aspects of a dendritic polymer.

Figure 5 shows the variation of the mean radius of gyration with molecular weight for linear and dendritic polymers. The circles are for the linear polymers; the squares are for generation-two dendrimers; the triangles are for generation-three dendrimers; the diamonds are for generation-four dendrimers; and the crosses are for generation-five dendrimers. As the generation number rises, the polymer becomes more compact. For dendritic polymers, the slope of the line giving the mean-square radius of gyration as a function of polymer molecular weight appears to be similar to that for linear polymers.

Polymer-Polymer Interactions

At a center-to-center distance, r, the potential of mean force between two molecules, $w(r)$, is the difference in the Helmholtz energy when the molecules are separated by r and that when they are infinitely far apart.

$$w(r) = A(r) - A(\infty)$$

$$= [U(r) - TS(r)] - [U(\infty) - TS(\infty)]$$
$$= -k_B T \ln \frac{\Omega(r)}{\Omega(\infty)} \quad (1)$$

The last relation follows because, for non-attracting polymers, $U(r) = U(\infty) = 0$ and because $S = k_B \ln \Omega$, where $\Omega(r)$ is the number of configurations available to the molecules when they are separated by distance r. Dautenhahn and Hall have used Eq. (1) to calculate the potential of mean force between linear chains.[20]

Simulations performed for pairs of polymer molecules at various separations yield the intermolecular correlation functions between polymer segments, the potential of mean force between polymer molecules, and the second virial coefficient. These simulations provide information on the behavior of polymer solutions at low concentrations.

Figure 6 shows the potential of mean force between linear chains with 91 segments (solid line) and that for third-generation dendrimers with $n = 3$ (dashed line).

Figure 7 shows the potential of mean force for second-generation dendrimers. The solid line is for $n = 2$; the dashed line is for $n = 5$; and the dotted line is for $n = 10$.

At low polymer concentrations, the osmotic pressure of a solution can be written as a virial series in the polymer concentration, c_2,

$$\beta\Pi = c_2 + B_2 c_2^2 + \cdots \quad (2)$$

where $\beta = (k_B T)^{-1}$, where k_B is the Boltzmann constant, and B_2 is the second virial coefficient, given by

$$B_2 = -2\pi \int d\omega_1 d\omega_2 dr_{12} r_{12}^2 \{\exp[-\beta U(1,2)] - 1\} \quad (3)$$

where ω_1 and ω_2 denote the conformation of polymer 1 and 2, respectively, r_{12} denotes the separation between the center of masses of the two polymer molecules, and U is the interaction energy between the two molecules.

Figure 8 shows how the second virial coefficient depends on the polymer molecular weight for linear and dendritic polymers. The circles are for linear polymers; the squares are for second-generation dendrimers; and the triangles are for third-generation dendrimers.

Integral-Equation Theory for the Polymer Solution

To obtain thermodynamic properties of dilute polymer solutions, we assume that the interaction between two polymer molecules is not affected by the presence of other polymer molecules. This approximation becomes exact at extremely low polymer concentrations. However, it becomes increasingly poor as the polymer concentration increases.

We use our potentials of mean force in conjunction with integral-equation theory for simple fluids.[22,23] We solve the Ornstein-Zernike equation with the Percus-Yevick approximation. The Ornstein-Zernike equation is

$$\hat{h}(q) = \hat{c}(q) + \hat{c}(q)\rho\hat{h}(q) \quad (4)$$

where h is the total correlation function, c is the direct correlation function, and ρ is the number density of molecules in the system. The $\hat{}$ designates a function's Fourier transform.

An approximate closure, appropriate for systems with only short-range repulsions, is the Percus-Yevick closure, given by

$$1 + h(r) = \exp[-\beta u(r)][1 + h(r) - c(r)] \tag{5}$$

where $u(r)$ is the interaction potential between two molecules. This approximation yields the exact second virial coefficient of the simple fluid.[22] To describe polymer molecules, we replace the interaction potential, $u(r)$, with the potential of mean force between polymer molecules, $w(r)$, which we described in the previous section.

The Ornstein-Zernike equation with the Percus-Yevick closure was solved numerically using the Gillan method.[24] We use a grid with $N = 2048$ points, and a grid spacing of $0.05R_g$. The pressure of the polymer system was computed by integrating the compressibility equation.

This calculation provides polymer-solution properties that are valid at high dilutions but become increasingly inaccurate as the polymer concentration increases. To estimate the range of applicability of this approximation, Figure 9 compares integral-equation calculations for a linear chain with $M = 51$ spheres with results of Monte-Carlo simulations. The squares indicate Monte-Carlo simulations[25] and the line is from integral-equation theory. Figure 9 shows that integral-equation theory is valid only for polymer concentrations less than about 0.1 packing fraction.

The approximation used here should be more accurate for compact molecules such as dendrimers. Figure 10 shows the predicted pressure as a function of polymer concentration for polymers composed of $M = 91$ spheres. The solid line is for a third-generation dendrimer with separator length $n = 2$, and the dashed line is for a linear polymer.

At very low polymer concentrations, we see that the pressure of the dendritic-polymer system is lower than that of the linear-polymer system. This is expected, since the dendrimer has a lower second virial coefficient. However, as the polymer concentration increases, more and more of the polymers begin to overlap. As overlappling becomes important, the pressure of the dendritic-polymer solution increases dramatically because the dendrimers are somewhat impenetrable. This dramatic increase is not seen in the linear polymers because they can more easily interpenetrate.

III. CONCENTRATED NON-ATHERMAL POLYMER SOLUTIONS

For concentrated polymer solutions, we place the polymer solution on a lattice with N_l total sites. Each site has z nearest neighbors. Each solvent molecule is assumed to occupy one lattice site, while each polymer molecule is assumed to occupy M lattice sites. In addition, the lattice is assumed to be fully occupied and, therefore, incompressible.

The volume fraction of polymer in solution, ϕ_2, is given by

$$\phi_2 = N_2 M / N_l \tag{6}$$

where N_2 is the number of polymer molecules in the system.

Attractive interactions in the system are characterized by parameter ϵ, given by

$$\epsilon = \epsilon_{11} + \epsilon_{22} - 2\epsilon_{12} \tag{7}$$

where ϵ_{11} is the energy of a solvent-solvent contact, ϵ_{22} is the energy of a nonbonded polymer segment-segment contact, and ϵ_{12} is the energy of a polymer segment-solvent contact. Subscript 1 refers to the solvent and subscript 2 refers to the polymer.

LATTICE-CLUSTER THEORY

Freed and coworkers have developed a lattice-cluster theory (LCT), for homogeneous polymers. In this theory, the Helmholtz energy of the system is expanded in a double power series in $1/z$ and $\beta\epsilon$. We truncate the series at fourth order in $1/z$ and second order in $\beta\epsilon$. Details of our calculations are given in the Appendix.

Thermodynamic Properties

We examine solutions of two homogeneous polymers: linear and dendritic. Figure 11 presents a schematic of polymer structure. The linear polymers are characterized by a single parameter, n, the total number of bonds ($M = n + 1$), as indicated in part (a). The dendritic polymers consist of a central core with three arms; an example is given in part (b). The dendrimer is characterized by two parameters, g, the generation number and, n, the number of bonds between branch points. Table 1 gives the counting indices for these types of polymers.

We first compute the vapor pressure of a homogeneous polymer-solvent mixture. The solvent chemical potential is related to the solution vapor pressure p by

$$\frac{p}{p^*} = \exp[\beta\Delta\mu_1] \tag{8}$$

where p^* is the vapor pressure of pure solvent at system temperature.

Figure 12 shows the solvent activity for solutions of polymers with $M = 466$ segments dissolved in a good solvent (i.e., $\epsilon = 0$). The solid line is from lattice-cluster theory (LCT) for a linear polymer ($n = 465$); the dashed line is from LCT for a dendritic polymer with $g = 4$ and $n = 2$; and the dotted line is from the Flory-Huggins theory. There is a large deviation between results from Flory-Huggins theory and those from LCT. However, results for the linear and dendritic polymer solutions are almost indistinguishable.

Figure 13 shows solvent activity for solutions of polymers with $M = 465$ segements at $k_BT/\epsilon = 3$. The legend is the same as that in Figure 12. At these conditions, the system shows liquid-liquid phase separation. Again, results from Flory-Huggins theory differ from those using LCT, and the results for linear and dendritic polymers are almost identical.

Figure 14 shows the liquid-liquid coexistence curve for solutions of polymers with $M = 466$ segments. The solid line is from LCT for the linear chain ($n = 465$); the dashed line is

from LCT for dendritic polymer ($g = 4$ and $n = 2$), and the dotted line is from Flory-Huggins theory.

The Flory-Huggins theory gives a much higher critical temperature for the polymer-solvent system than LCT. However, it is well-known that the Flory-Huggins theory over-predicts the coexistence curve in the vicinity of the critical point.[26] LCT indicates that the dendritic-polymer solutions have a slightly lower critical point than those of the linear polymer solutions, i.e., the dendrimer is slightly more soluble than the corresponding linear polymer. At low temperatures, results from Flory-Huggins theory merge with those from LCT for linear and dendritic polymers.

Figure 15 shows the variation of the critical temperature of linear and dendritic-polymer solutions as a function of molecular weight. The difference between results for linear and dendritic polymers rises as the molecular weight of the polymer increases and as the spacer length of the dendrimer decreases.

According to Flory,[16] the thermodynamic properties of concentrated polymers should depend only weakly on polymer architecture. Because the polymer solution is concentrated, each polymer segment is in close contact with several other polymer segments. The properties of the solution at these conditions are governed primarily by excluded-volume interactions between polymer segments, and therefore the connectivity of the polymer segments plays an insignificant role.

This argument, however, assumes that the polymer molecules interpenetrate. This may not be the case for dendritic polymers of high generation number. If the dendrimers do not interpenetrate, each segement sees a different environment in the solution, depending on where it is located in the dendrimer. Thus, architecture plays a greater role in determining the solution's thermodynamic properties.

Because the LCT used here is truncated after a finite number of terms, it only accounts for short range correlations between polymer segments. It is the long-range correlations of the dendritic polymer (i.e., interactions between segments located in distant parts on the same molecule) which cause it to be impenetrable. Therefore, the predictions of the LCT should be regarded with caution, especially for higher-generation dendrimers.

IV. CONCLUSIONS

From our simulations of single homogeneous dendritic polymers, we find that the center of a dendritic polymer is not hollow. For low-generation dendrimers, there is a shoulder in the segment density profile from about $r = R_g/2$ to $r = R_g$ due to the architecture of the dendrimer. For higher-generation dendrimers, this shoulder is a local maximum. These results agree with previous simulations of other workers.[13–15] We find that the shoulder becomes more pronounced as the separator length of the dendrimer decreases.

The qualitative difference between the segment density profiles obtained from computer simulations and those from self-consistent mean-field calculations suggests that the properties of dendritic polymers may not be amenable to a simple mean-field analysis.

Dendritic polymers are less penetrable than linear polymers, as indicated by their more repulsive potential of mean force. However, as the separator length increases, the dendrimers become more penetrable.

LCT calculations indicate that the liquid-liquid coexistence curve for a homogeneous-dendritic-polymer solution is slightly lower than that for a linear-polymer solution. This difference in the critical solution temperature rises with increasing generation number and decreasing separator length.

All the results given in this work are for homogeneous polymers, i.e. polymers with identical segments. However, dendrimers for interesting applications are not homogeneous; in a typical real dendrimer, segments at the periphery are chemically different from those inside. Therefore, while the results of this work provide a useful first step toward understanding solutions of dendrimers, they are not yet directly applicable to most dendrimers that are promising for technology.

ACKNOWLEDGEMENTS

This work was supported by the Director, Office of Energy Research, Office of Basic Energy Sciences, Chemical Sciences Division of the U.S. Department of Energy under Contract No. DE-AC03-76SF0098.

APPENDIX.

In lattice cluster theory (LCT), polymer architecture is characterized by a set of seven parameters, known as counting indicies: M, $N^{(1)}$, $N^{(2)}$, $N^{(3)}$, $N^{(\perp)}$, $N^{(1,1)}$, and $N^{(1,2)}$. M is the number of segments in each molecule. $N^{(1)}$ is the number of bonds in each molecule. $N^{(2)}$ is the number of consecutive bonds. $N^{(3)}$ is the number of ways three consecutive bonds can be chosen. $N^{(\perp)}$ is the number of ways in which three bonds intersect. $N^{(1,1)}$ is the number of nonconsecutive bonds. $N^{(1,2)}$ is the number of ways in which a single bond and a consecutive pair of bonds, which do not intersect the single bond, can be chosen.

The Helmholtz energy of mixing is given by[26]

$$\Delta A = \Delta A^{ath} + \Delta A^{int} \tag{A1}$$

where ΔA^{ath} is the Helmholtz energy of mixing of an athermal solution, and ΔA^{int} is the contribution of attractive interactions.

$$\begin{aligned}\frac{\beta \Delta A^{ath}}{N_l} = \frac{\phi_2}{M}\ln\phi_2 + (1-\phi_2)\ln(1-\phi_2) \\ +a^{(0)}\phi_2(1-\phi_2) + a^{(1)}\phi_2^2(1-\phi_2) + a^{(2)}\phi_2^3(1-\phi_2)\end{aligned} \tag{A2}$$

where $a^{(i)}$ are parameters that depend only on the architecture of the polymer molecule.

$$\begin{aligned}a^{(0)} &= \frac{1}{z}[K^{(1)}]^2 + \frac{1}{z^2}[-4K^{(1)}K^{(2)} + \frac{8}{3}[K^{(1)}]^3 - 2K^{(1)}K^{(3)} + [K^{(2)}]^2 \\ &\quad -2K^{(1)}(K^{(1,2)} - K^{(1)}K^{(2)}M) + 2[K^{(1)}]^4 \\ &\quad +2[K^{(1)}]^2(K^{(1,1)} - [K^{(1)}]^2M) - 6K^{(1)}K^{(\perp)}] \\ a^{(1)} &= \frac{1}{z^2}[\frac{8}{3}[K^{(1)}]^3 + 2[K_1]^4 + 2[K^{(1)}]^2(K^{(1,1)} - [K^{(1)}]^2M)] \\ a^{(2)} &= \frac{1}{z^2}2[K^{(1)}]^4\end{aligned} \tag{A3}$$

$$\begin{aligned}\frac{\beta \Delta A^{int}}{N_l} &= A^{(1)}\phi_2(1-\phi_2) + (A^{(2)} + B^{(3)})\phi_2^2(1-\phi_2)^2 \\ &\quad +A^{(3)}\phi_2^2(1-\phi_2)^2(1-2\phi_2)^2 \\ &\quad +A^{(4)}\phi_2^2(1-\phi_2)^2[1-6\phi_2(1-\phi_2)(3\phi_2^2-3\phi_2+2)] \\ &\quad +(B^{(1)} + B^{(2)})\phi_2(1-\phi_2)^2 \\ &\quad +B^{(4)}\phi_2^3(1-\phi_2)^2 \\ &\quad +C^{(1)}\phi_2(1-\phi_2)^2(1-2\phi_2)^2 \\ &\quad +C^{(2)}\phi_2(1-\phi_2)^3 \\ &\quad +C^{(3)}\phi_2^2(1-\phi_2)^3(1-3\phi_2) \\ &\quad +C^{(4)}\phi_2(1-\phi_2)^4\end{aligned} \tag{A4}$$

$$A^{(1)} = \frac{\beta\epsilon z}{2} \tag{A5}$$

$$A^{(2)} = -\frac{(\beta\epsilon)^2 z}{4} \tag{A6}$$

$$A^{(3)} = -\frac{(\beta\epsilon)^3 z}{12} \tag{A7}$$

$$A^{(4)} = -\frac{(\beta\epsilon)^4 z}{48} \tag{A8}$$

$$B^{(1)} = -\beta\epsilon K_1 \tag{A9}$$

$$B^{(2)} = \frac{\epsilon}{z}(2K^{(2)} + K^{(3)} + 3K^{(\perp)} + K^{(1,2)} - K^{(1)}K^{(2)}M) \tag{A10}$$

$$B^{(3)} = -\frac{2\beta\epsilon}{z}K^{(1)}(2K^{(1)} + K^{(1,1)} - [K^{(1)}]^2 M) \tag{A11}$$

$$B^{(4)} = -\frac{4\beta\epsilon}{z}[K^{(1)}]^3 \tag{A12}$$

$$C^{(1)} = -\frac{(\beta\epsilon)^2}{2}K^{(1)} \tag{A13}$$

$$C^{(2)} = -(\beta\epsilon)^2 K^{(2)} \tag{A14}$$

$$C^{(3)} = -(\beta\epsilon)^2[K^{(1)}]^2 \tag{A15}$$

$$C^{(4)} = -\frac{(\beta\epsilon)^2}{2}(K^{(1,1)} - [K^{(1)}]^2 M) \tag{A16}$$

where $K^{(i)} = N^{(i)}/M$ (i = 1, 2, 3, or $\perp$) and $K^{(i,j)} = N^{(i,j)}/M$ (i = 1, or 2).

Upon mixing, the change in chemical potential of the solvent, $\Delta\mu_1$, can be determined from the Helmholtz energy,

$$\begin{aligned}\Delta\mu_1 &= \frac{\partial \Delta A}{\partial N_1} \\ &= \frac{\Delta A}{N_l} - \phi_2 \frac{\partial \Delta A/N_l}{\partial \phi_2} \\ &= \Delta\mu_1^{ath} + \Delta\mu_1^{int}\end{aligned} \tag{A17}$$

where

$$\begin{aligned}\beta\Delta\mu_1^{ath} = \ln(1-\phi_2) + (1-\frac{1}{M})\phi_2 \\ +a^{(0)}\phi_2^2 - a^{(1)}\phi_2^2(1-2\phi_2) - a^{(2)}\phi_2^3(2-3\phi_2)\end{aligned} \tag{A18}$$

and

$$\begin{aligned}\beta\Delta\mu_1^{int} = A^{(1)}\phi_2^2 - (A^{(2)} + B^{(3)})\phi_2^2(1-\phi_2)(1-3\phi_2) \\ -A^{(3)}\phi_2^2(1-\phi_2)(1-2\phi_2)(1-9\phi_2+10\phi_2^2)\end{aligned}$$

$$
\begin{aligned}
&-A^{(4)}\phi_2^2(1-\phi_2)(1-27\phi_2+138\phi_2^2-294\phi_2^3+306\phi_2^4-126\phi_2^5)\\
&+(B^{(1)}+B^{(2)})2\phi_2^2(1-\phi_2)\\
&-B^{(4)}2\phi_2^3(1-\phi_2)(1-2\phi_2)\\
&-C^{(1)}2\phi_2^2(1-\phi_2)(1-2\phi_2)(3-4\phi_2)\\
&+C^{(2)}3\phi_2^2(1-\phi_2)^2\\
&-C^{(3)}\phi_2^2(1-\phi_2)^2(1-10\phi_2+15\phi_2^2)\\
&+C^{(4)}4\phi_2^2(1-\phi_2)^3
\end{aligned}
\tag{A19}
$$

Upon mixing, the change in chemical potential of the polymer, $\Delta\mu_2$, can be determined from the Helmholtz energy,

$$
\begin{aligned}
\Delta\mu_2 &= \frac{\partial\Delta A}{\partial N_2}\\
&= \frac{\Delta A}{N_l}+(1-\phi_2)\frac{\partial\Delta A/N_l}{\partial\phi_2}\\
&= \Delta\mu_2^{ath}+\Delta\mu_2^{int}
\end{aligned}
\tag{A20}
$$

where

$$
\begin{aligned}
\frac{1}{M}\beta\Delta\mu_2^{ath} = \ln\phi_2 &- (1-\frac{1}{M})(1-\phi_2)\\
&+a^{(0)}(1-\phi_2)^2+a^{(1)}2\phi_2(1-\phi_2)^2+a^{(2)}3\phi_2^2(1-\phi_2)^2
\end{aligned}
\tag{A21}
$$

and

$$
\begin{aligned}
\beta\Delta\mu_2^{int} = &A^{(1)}(1-\phi_2)^2+(A^{(2)}+B^{(3)})\phi_2(1-\phi_2)^2(2-3\phi_2)\\
&+A^{(3)}\phi_2(1-\phi_2)^2(1-2\phi_2)(2-11\phi_2+10\phi_2^2)\\
&+A^{(4)}\phi_2(1-\phi_2)^2(2-39\phi_2+168\phi_2^2-330\phi_2^3+324\phi_2^4-126\phi_2^5)\\
&+(B^{(1)}+B^{(2)})(1-\phi_2)^2(1-2\phi_2)\\
&+B^{(4)}\phi_2^2(1-\phi_2)^2(3-4\phi_2)\\
&+C^{(1)}(1-\phi_2)^2(1-2\phi_2)(1-8\phi_2+8\phi_2^2)\\
&+C^{(2)}(1-\phi_2)^3(1-3\phi_2)\\
&+C^{(3)}\phi_2(1-\phi_2)^3(1-5\phi_2)(2-3\phi_2)\\
&+C^{(4)}(1-\phi_2)^4(1-4\phi_2)
\end{aligned}
\tag{A22}
$$

REFERENCES

1. Tomalia, D. A.; Naylor, A. M.; Goddard, III, W. A. *Angew. Chem. Int. Ed. Engl.* **1990**, *29*, 138.

2. Dagani, R. *C&EN* **1996**, *June 3*, 30.

3. Tomalia, D. A.; Dvornic, P. R. *Nature*, **1994**, *372*, 617.

4. Hawker, C. J.; Wooley, K. L.; Fréchet, J. M. J. *J. Chem. Soc. Perkin Trans. 1* **1993**, 1287.

5. Newkome, G. R.; Moorefield, C. N.; Barker, G. R.; Johnson, A. L.; Behera, R. K. *Angew. Chem. Int. Ed. Engl.* **1991**, *30*, 1176.

6. Newkome, G. R.; Moorefield, C. N.; Barker, G. R.; Saunders, M. J.; Grossman, S. H. *Angew. Chem. Int. Ed. Engl.* **1991**, *30*, 1178.

7. Wiener, E. C.; Brechbiel, M. W.; Brothers, H.; Magin, R. L.; Gansow, O. A.; Tomalia, D. A.; Lauterbur, P. C. *Magnetic Resonance in Medicine* **1994**, 1.

8. de Gennes, P. G; Hervet, H. *J. Physique Lett.* **1983**, *44*, 351.

9. Biswas, P.; Cherayil, B. J. *J. Chem. Phys.* **1994**, *100*, 3201.

10. Boris, D.; Rubinstein, M. *Macromolecules* **1996**, *29*, 7251.

11. Lescanec, R. L.; Muthukumar, M. *Macromolecules* **1990**, *23*, 2280.

12. Naylor, A. M.; Goddard, III, W. A.; Kiefer, G. E.; Tomalia, D. *J. Am. Chem. Soc.* **1989**, *111*, 2339.

13. Mansfield, M. L.; Klushin, L. I. *Macromolecules* **1993**, *26*, 4262.

14. Murat, M.; Grest, G. S. *Macromolecules* **1996**, *29*, 1278.

15. Chen, Z. Y.; Cui, S.-M. *Macromolecules* **1996**, *29*, 7943.

16. Flory, P. J. *Principles of Polymer Chemistry*; Cornell University Press: Ithaca, 1953.

17. Guggenheim, E. A. *Mixtures: The Theory of the Equilibrium Properties of Some Simple Classes of Mixtures, Solutions, and Alloys*; Clarendon: Oxford, 1952, Ch. 10.

18. Nemirovski, A. M.; Bawendi, M. G.; Freed, K. F. *J. Chem. Phys.* **1987**, *87*, 7272. Freed, K. F.; Bawendi, M. G. *J. Phys. Chem.* **1989**, *93*, 2194. Dudowicz, J.; Freed, M. S.; Freed, K. F. *Macromolecules* **1991**, *24*, 5096. Freed, K. F.; Dudowicz, J. *Theor. Chim. Acta*, **1992**, *82*, 357.

19. Dudowicz, J.; Freed, K. F. *Macromolecules* **1991**, *24*, 5076. Nemirovski, A. M.; Dudowicz, J.; Freed, K. F. *Phys. Rev. A* **1992**, *45*, 7111.

20. Dautenhahn, J.; Hall, C. K. *Macromolecules* **1994**, *27*, 5399.

21. Escobedo, F. A.; de Pablo, J. J. *J. Chem. Phys.* **1995**, *102*, 2536. Escobedo, F. A.; de Pablo, J. J. *J. Chem. Phys.* **1996**, *104*, 4788.

22. Hansen, J. P; McDonald, I. R. *Theory of Simple Liquids*; Academic Press: London, 1986, 2ed.

23. Lee, L. L. *Molecular Thermodynamics of Nonideal Fluids*; Butterworths: Boston, 1988.

24. Gillan, M. J. *Mol. Phys.* **1979**, *38*, 1781.

25. Gao, J.; Weiner, J. H. *J. Chem. Phys.* **1989**, *91*, 3168.

26. Dudowicz, J.; Freed, K. F.; Madden, W. G. *Macromolecules* **1990**, *23*, 4803.

TABLES

TABLE I. Geometric parameters for linear and dendritic polymers.

	linear	dendrimer
M	$n+1$	$3(2^{g-1}-1)n+1$
$N^{(1)}$	n	$3(2^{g-1}-1)n$
$N^{(2)}$	$n-1$	$3(2^{g-1}-1)(n-1)+3N^{(\perp)}$
$N^{(3)}$	$n-2$	$3(2^{g-1}-1)(n-2)+6N^{(\perp)}$
$N^{(\perp)}$	0	$3(2^{g-2}-1)+1$
$N^{(1,1)}$	$(n-1)(n-2)/2$	$3(2^{g-1}-1)(n-1)(n-2)/2$ $+3(2^{g-1}-1)[3(2^{g-1}-1)-1]n^2/2-3N^{(\perp)}$
$N^{(1,2)}$	$(n-2)(n-3)$	$3(2^{g-1}-1)(n-2)(n-3)+3N^{(\perp)}(N^{(1)}-5)$ $+3(2^{g-1}-1)[3(2^{g-1}-1)-1]n(n-1)-6N^{(\perp)}$

FIGURE CAPTIONS

Figure 1: Schematic drawing of simulated polymer molecules: (a) linear, (b) dendritic.

Figure 2: Distribution of polymer segments from center of mass for: (i) linear polymer with 91 segments (solid line), (ii) third-generation dendrimer with $n = 2$ (dashed line).

Figure 3: Distribution of polymer segments from center of mass for second-generation dendrimers: (i) $n = 2$ (solid line), (ii) $n = 3$ (dashed line), (iii) $n = 4$ (dotted line), (iv) $n = 5$ (dashed-dotted line).

Figure 4: Distribution of polymer segments from center of mass for dendritic polymers with n=2: (i) second-generation dendrimer (solid line), (ii) third-generation dendrimer (dashed line), (iii) fourth-generation dendrimer (dotted line), (iv) fifth-generation dendrimer (dashed-dotted line).

Figure 5: Mean-square radius of gyration as a function of number of hard spheres: (i) linear chains (circles), (ii) second-generation dendrimers (squares), (iii) third-generation dendrimers (triangles), (iv) fourth-generation dendrimers (diamonds), (v) fifth-generation dendrimers (cross).

Figure 6: Potential of mean force for: (i) linear polymer with 91 segments (solid line), (ii) third-generation dendrimer with $n = 2$ (dashed line).

Figure 7: Potential of mean force for second-generation dendrimers: (i) $n = 2$, (solid line), (ii) $n = 5$ (dashed line), (iii) $n = 10$ (dotted line).

Figure 8: Second virial coefficient as a function of number of hard spheres in the polymer for: (i) linear chains (circles), (ii) second-generation dendrimers (squares), (iii) third-generation dendrimers (triangles), (iv) fourth-generation dendrimers (diamonds), (iv) fifth-generation dendrimers (cross).

Figure 9: Compressibility factor, Z, for tangent hard-sphere chains with $M = 51$: (i) Monte-Carlo simulations (circles), (ii) Percus-Yevick equation (line).

Figure 10: Pressure of tangent, hard-sphere polymers: (i) linear chain with $M = 91$ (solid line), (ii) third-generation dendrimer with a $n = 2$ (dashed line).

Figure 11: Schematic drawing for: (i) linear polymer, (ii) dendrimer.

Figure 12: Solvent activity in a good solvent: (i) linear polymer with $n = 465$ with LCT (solid line), (ii) dendritic polymer with $g = 4$ and $n = 2$ with LCT (dashed line), (iii) Flory-Huggins theory (dotted line).

Figure 13: Solvent activity at $k_BT/\epsilon = 3$: (i) linear polymer with $n = 465$ with LCT (solid line), (ii) dendritic polymer with $g = 4$ and $n = 2$ with LCT (dashed line), (iii) Flory-Huggins theory (dotted line).

Figure 14: Predicted liquid-liquid coexistence curve for: (i) linear polymer with $n = 465$ with LCT (solid line), (ii) dendritic polymer with $g = 4$ and $n = 2$ with LCT (dashed line), (iii) Flory-Huggins theory (dotted line).

Figure 15: Critical temperature as a function of polymer molecular weight for: (i) linear chains (open circles), (ii) dendrimers with $n = 2$ (squares), (iii) dendrimers with $n = 5$.

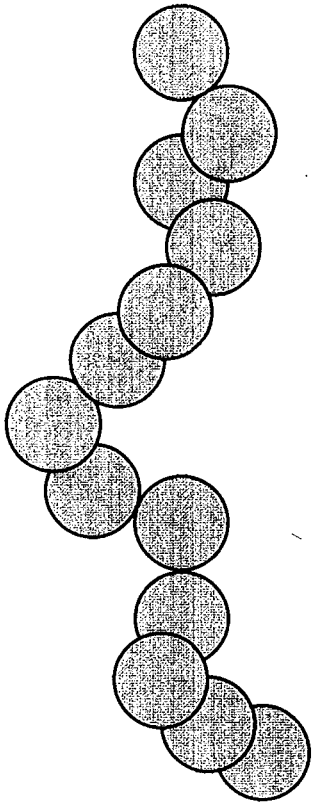

(a) linear chain

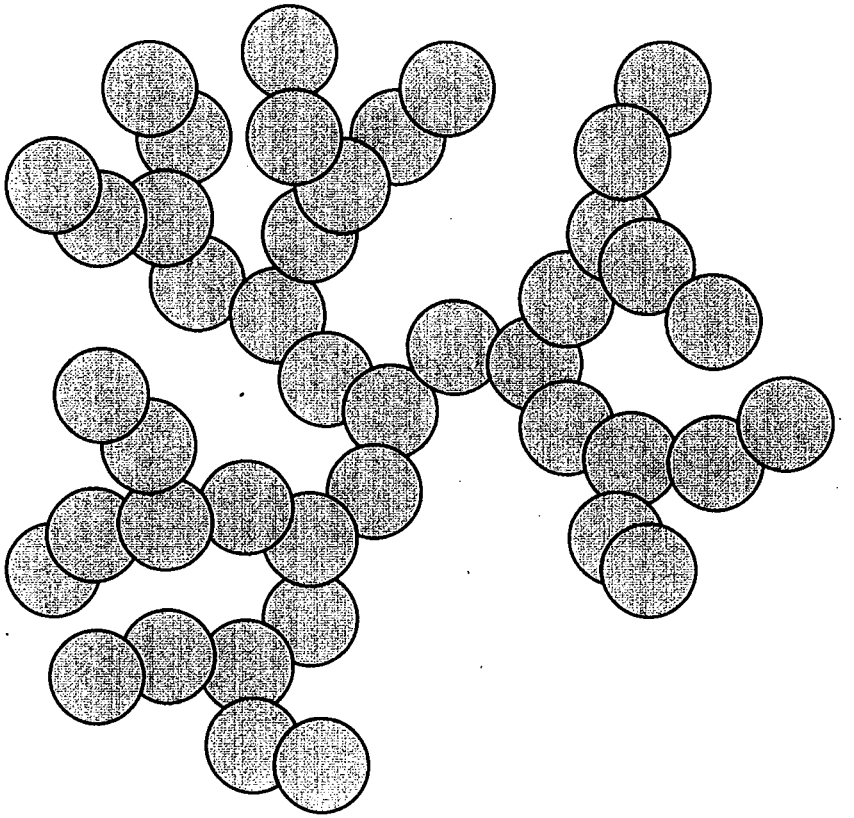

(b) dendrimer

Figure 1

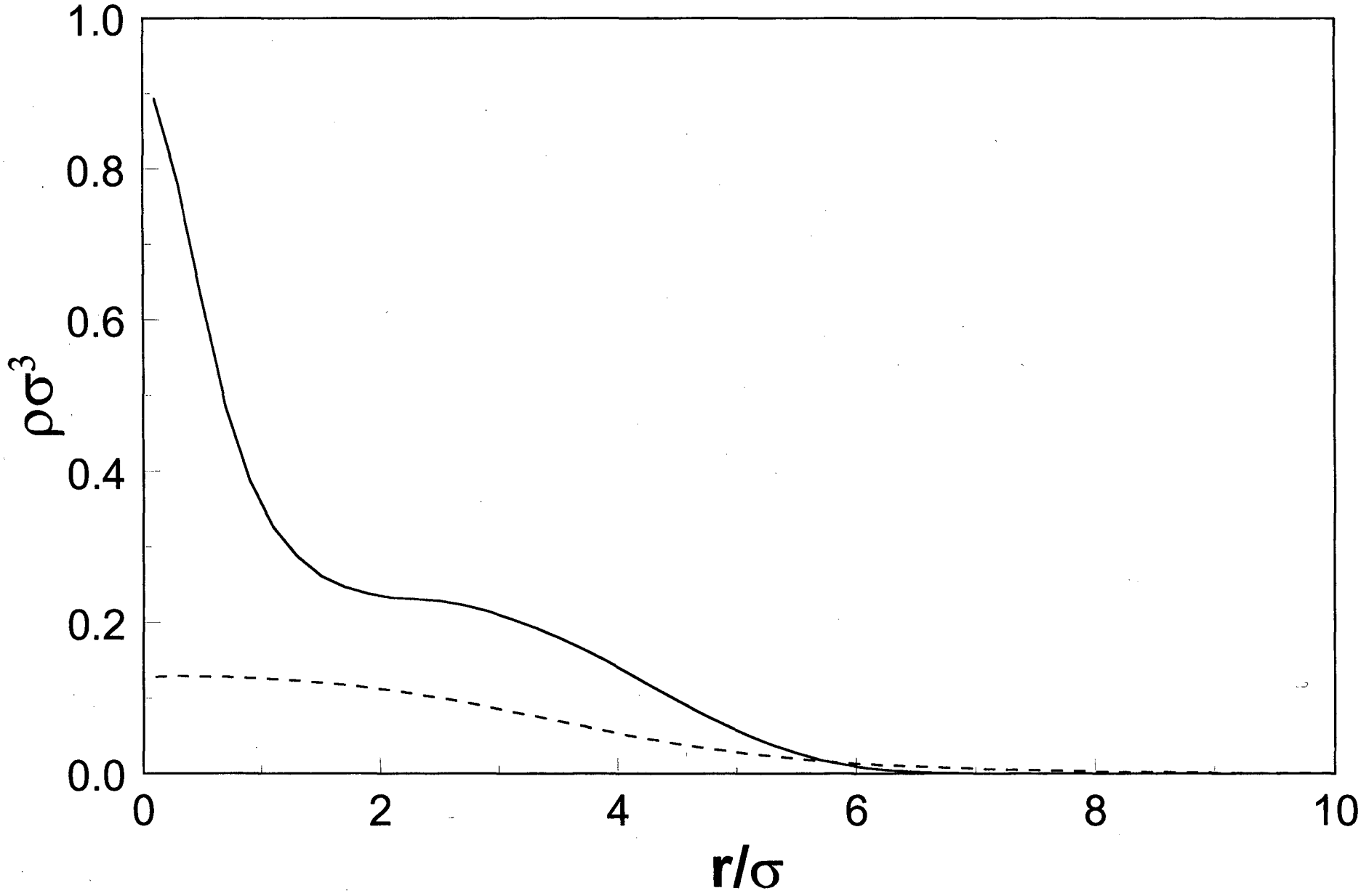

Figure 2

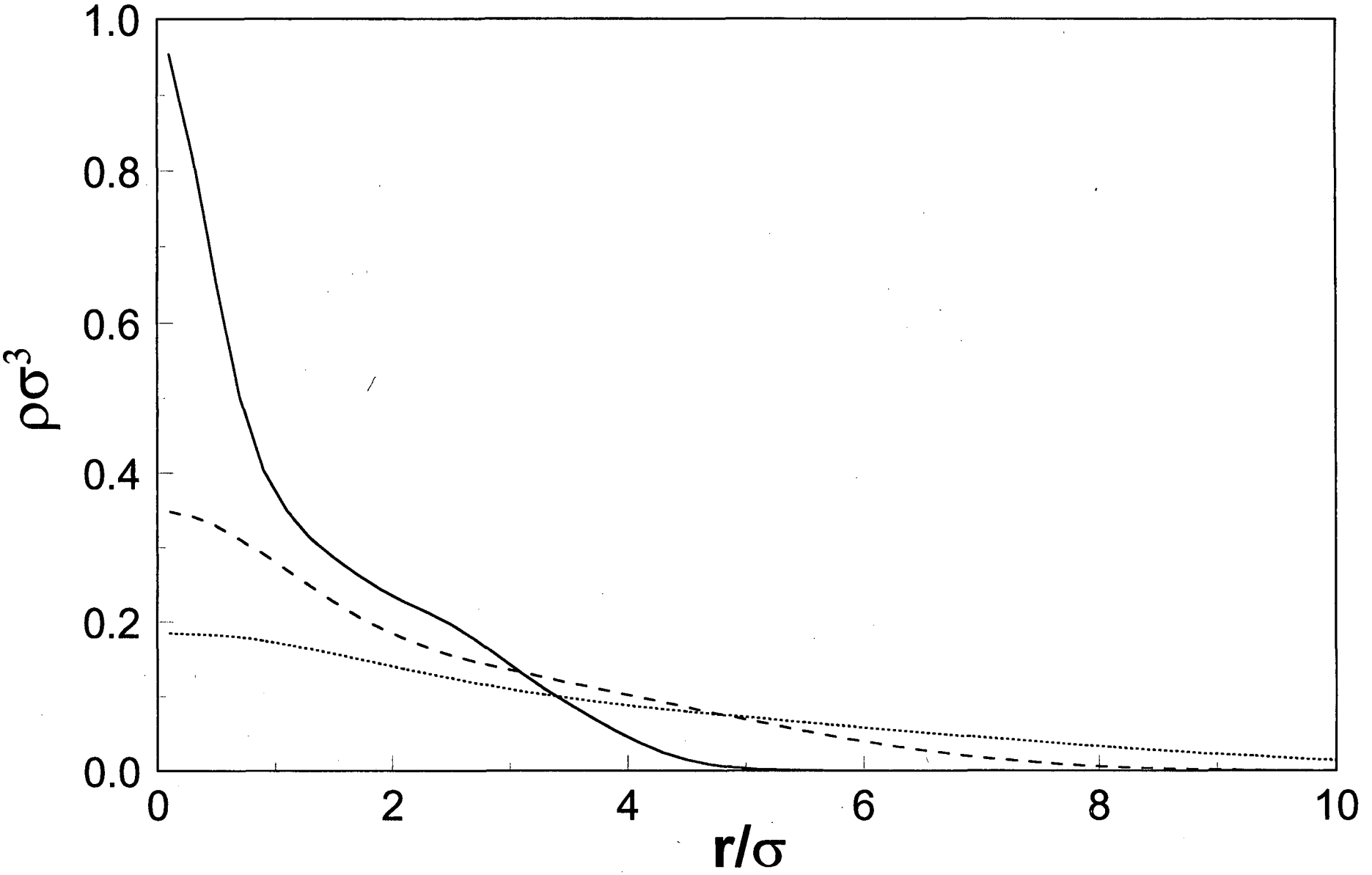

Figure 3

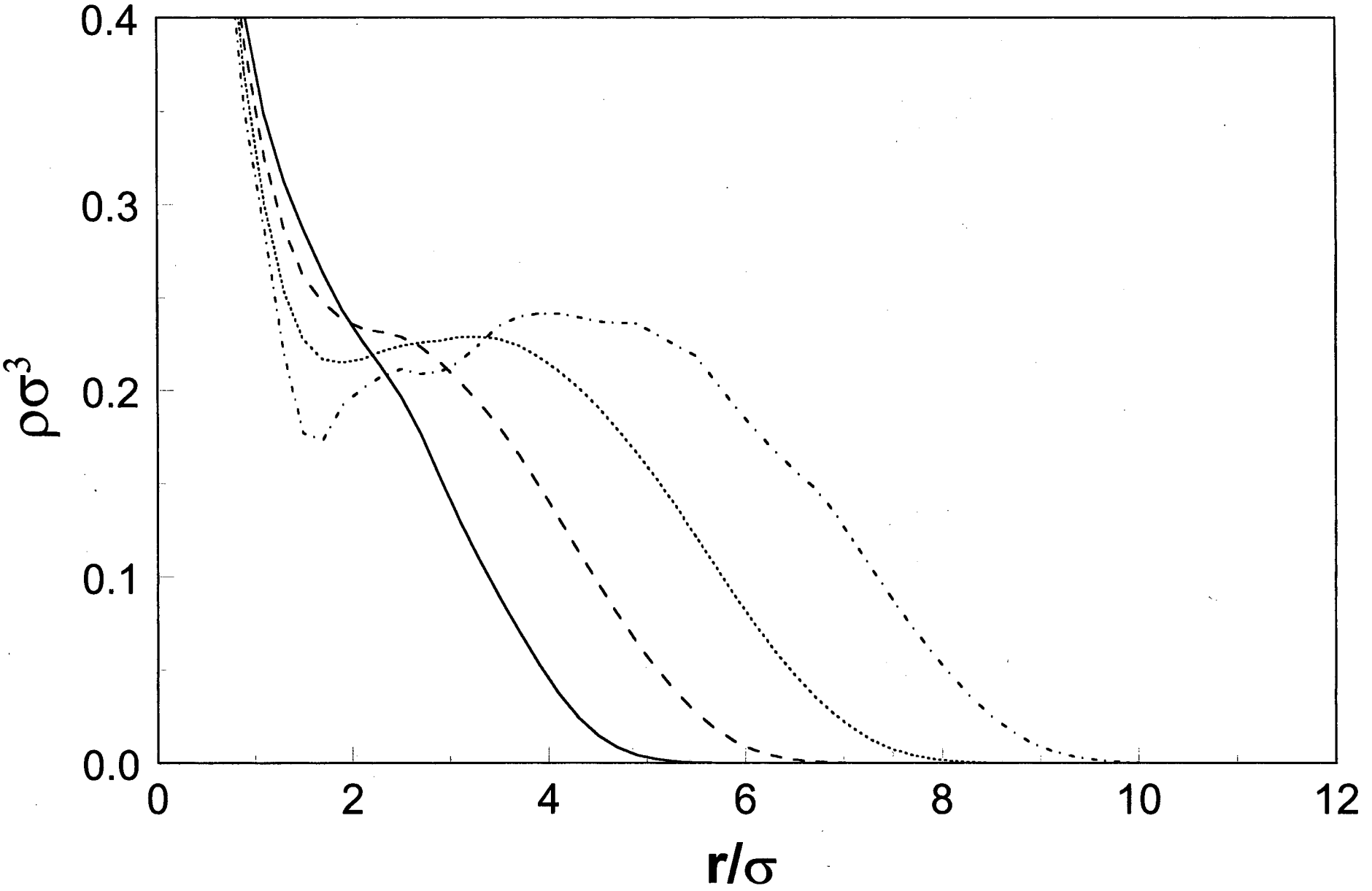

Figure 4

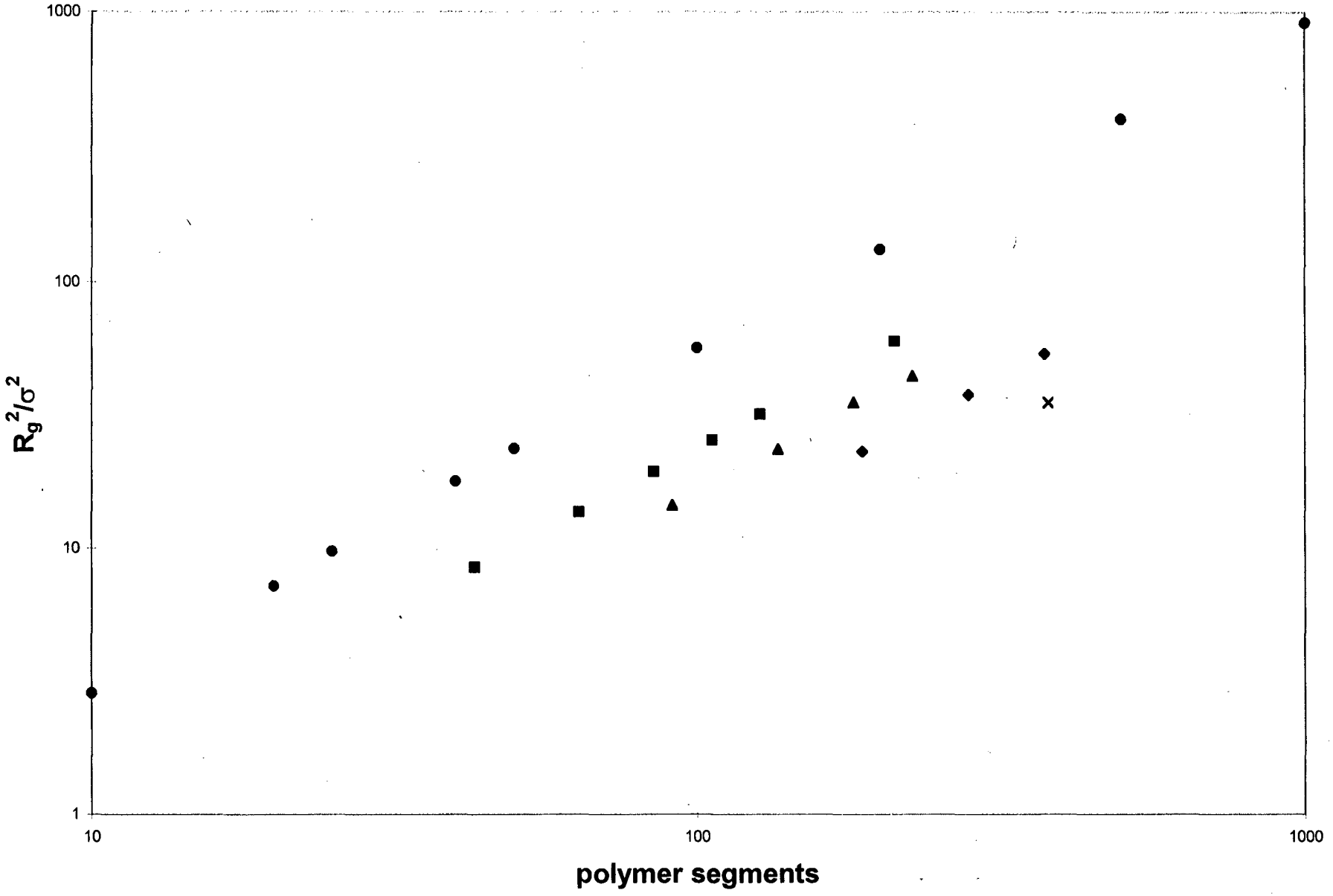

Figure 5

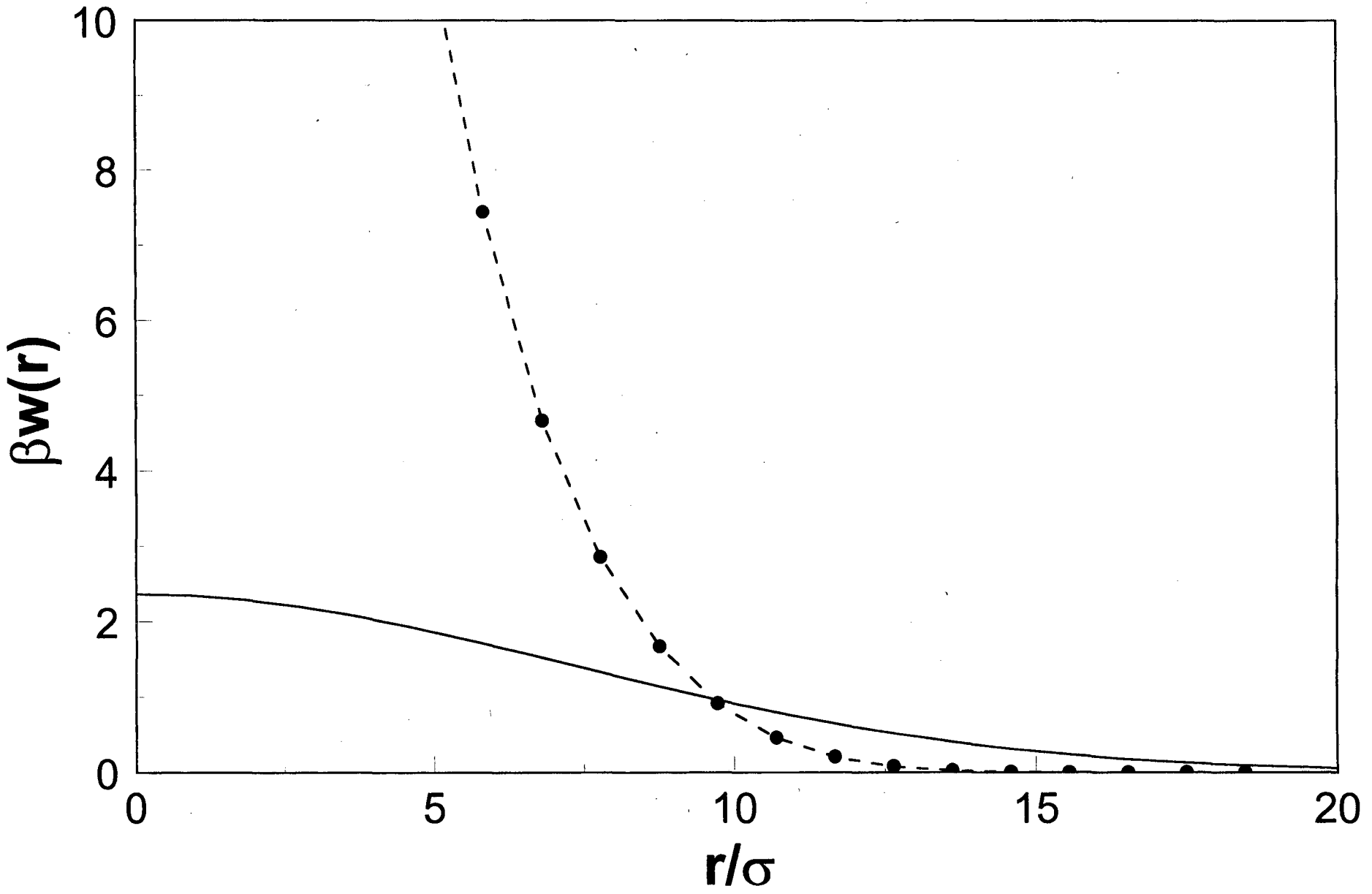

Figure 6

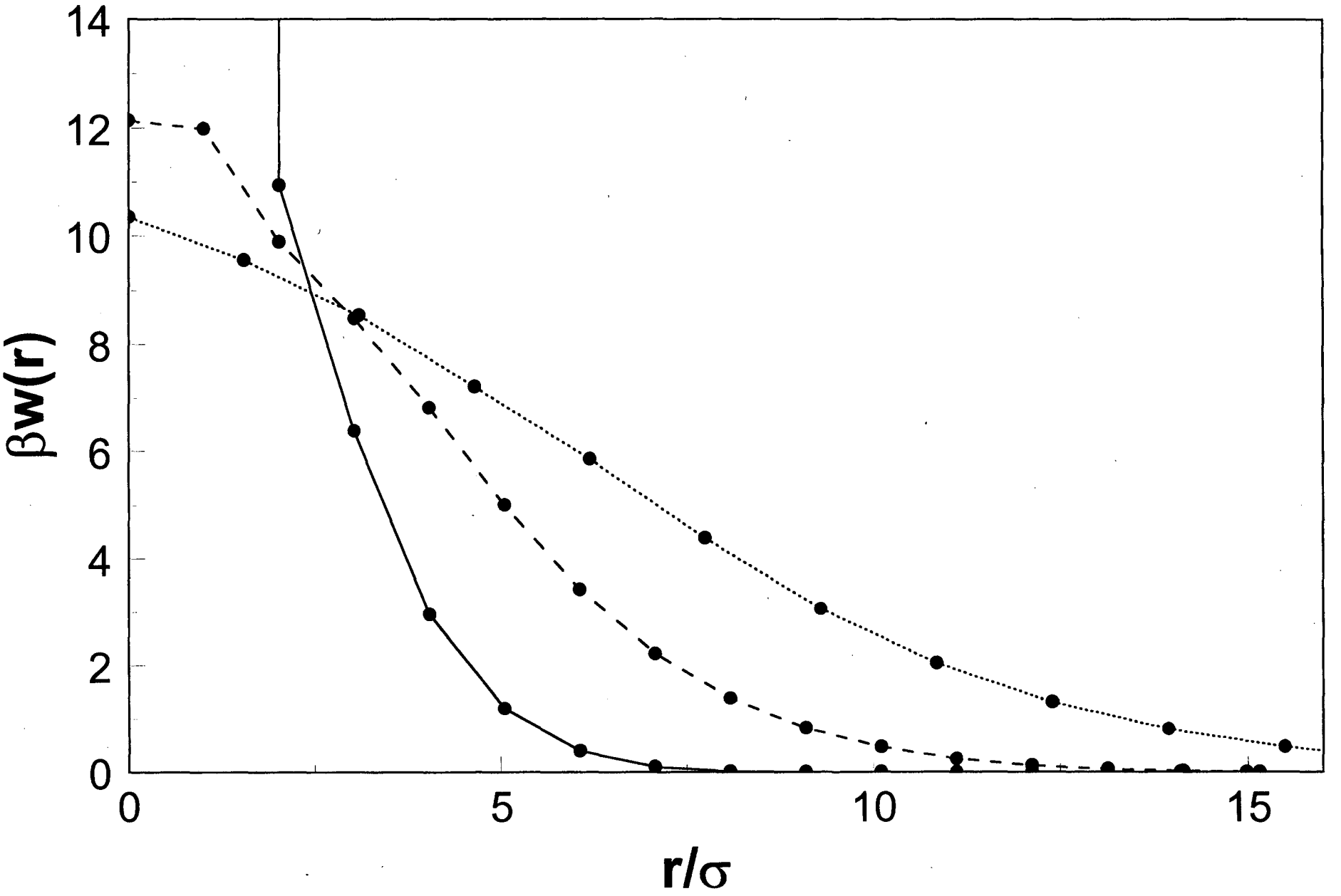

Figure 7

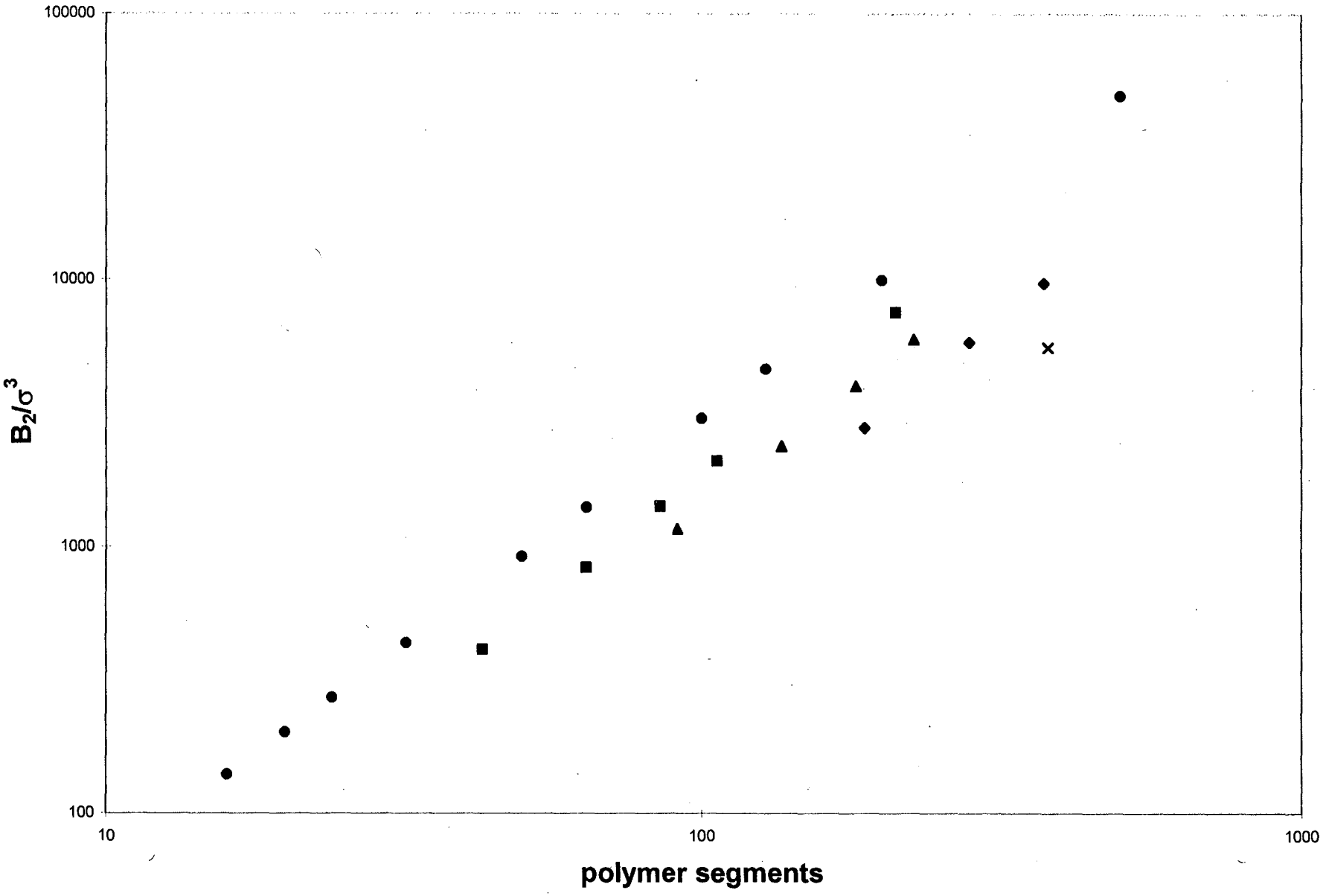
100000
10000
1000
100
B_2/σ^3
10
100
1000
polymer segments

Figure 8

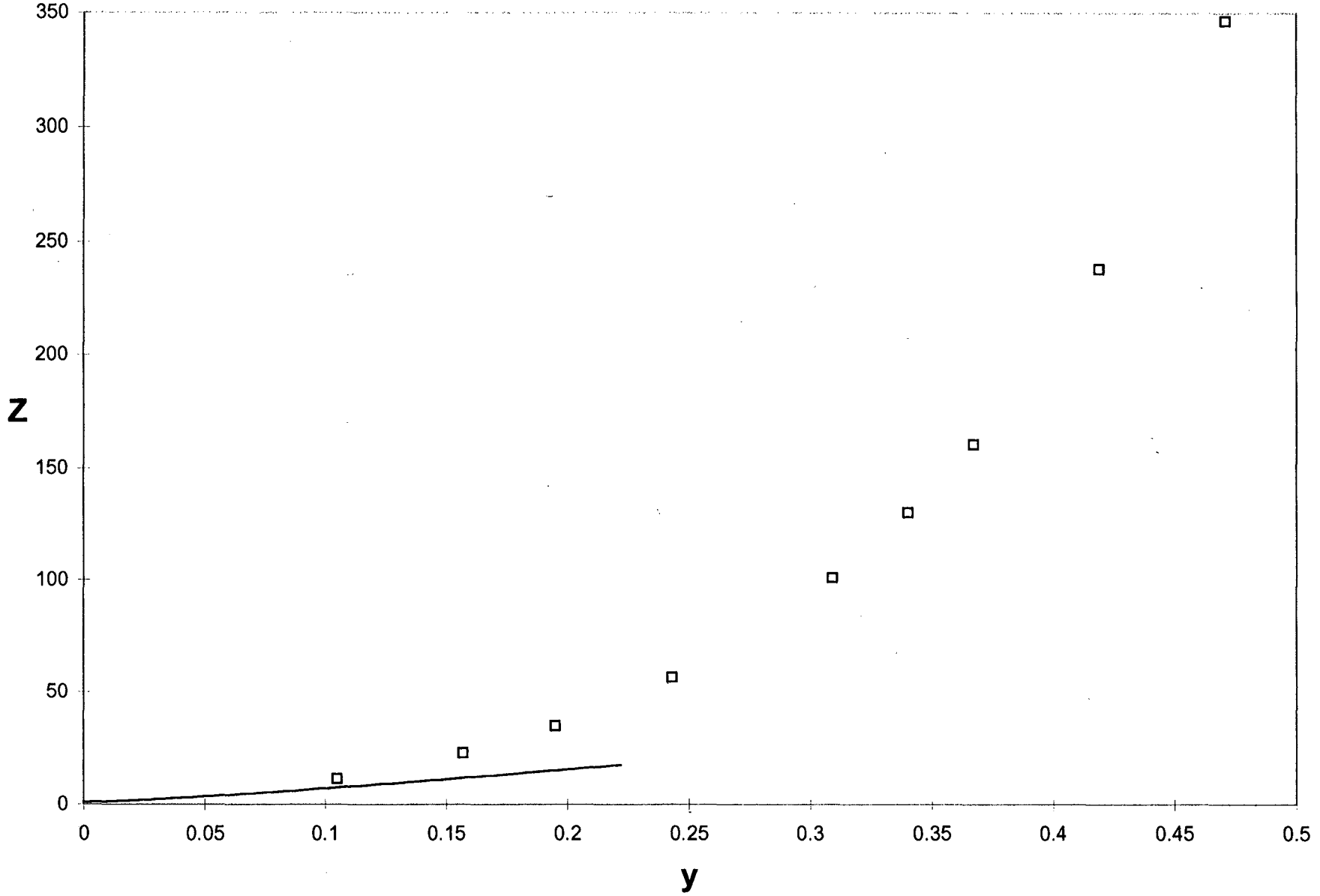

Figure 9

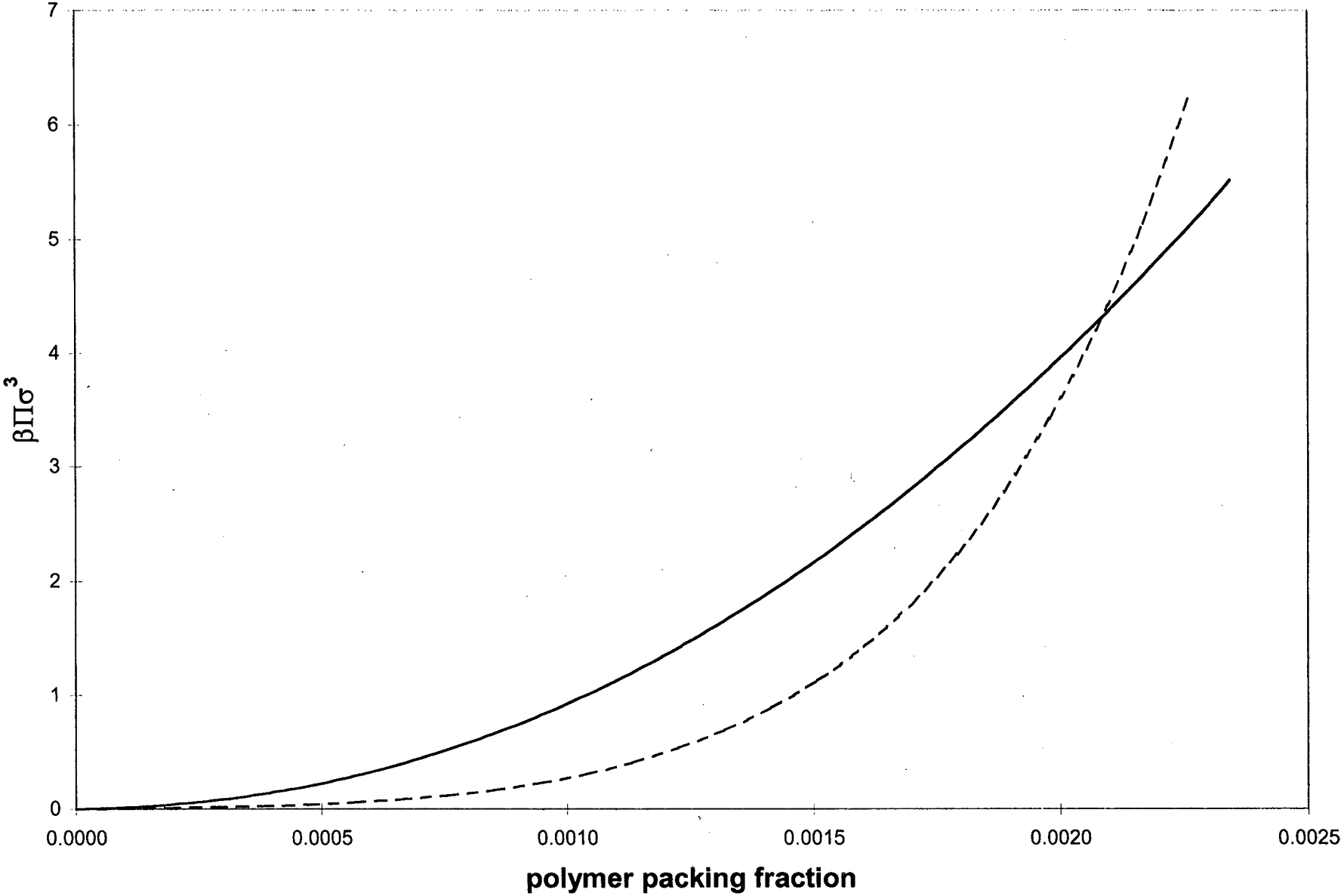
7
6
5
4
3
2
1
0
βΠσ3
0.0000
0.0005
0.0010
0.0015
0.0020
0.0025
polymer packing fraction

Figure 10

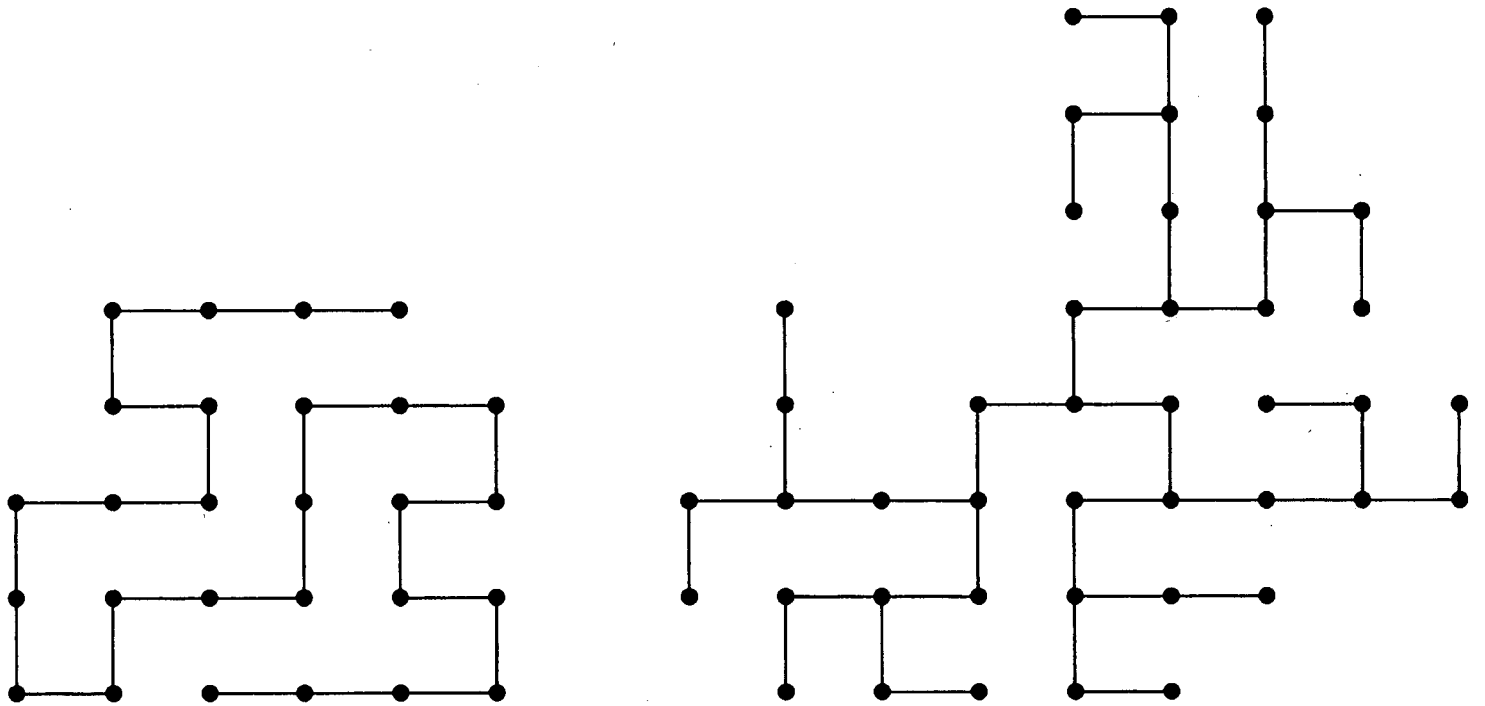

(a) linear chain (b) dendrimer

Figure 11

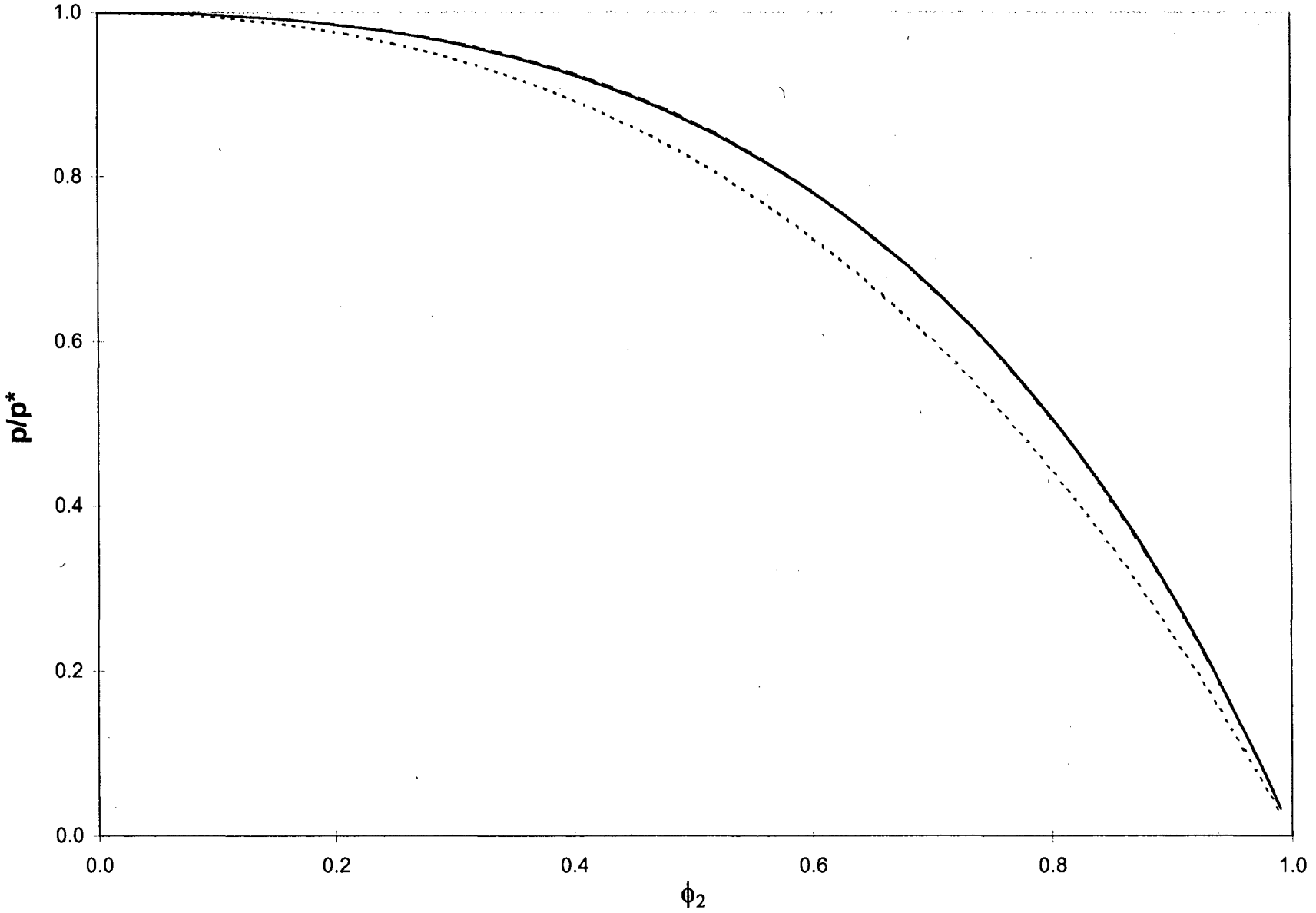

Figure 12

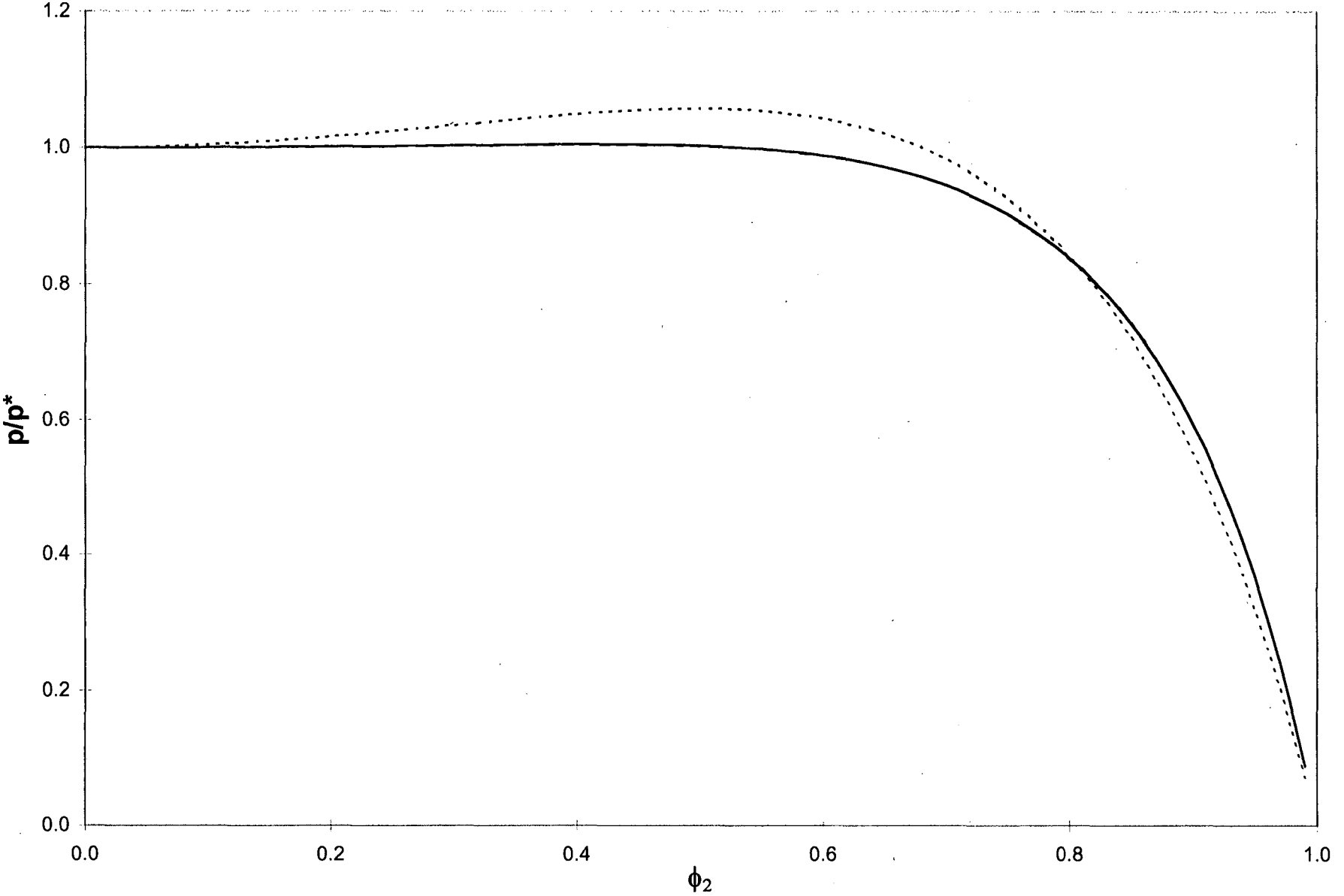

Figure 13

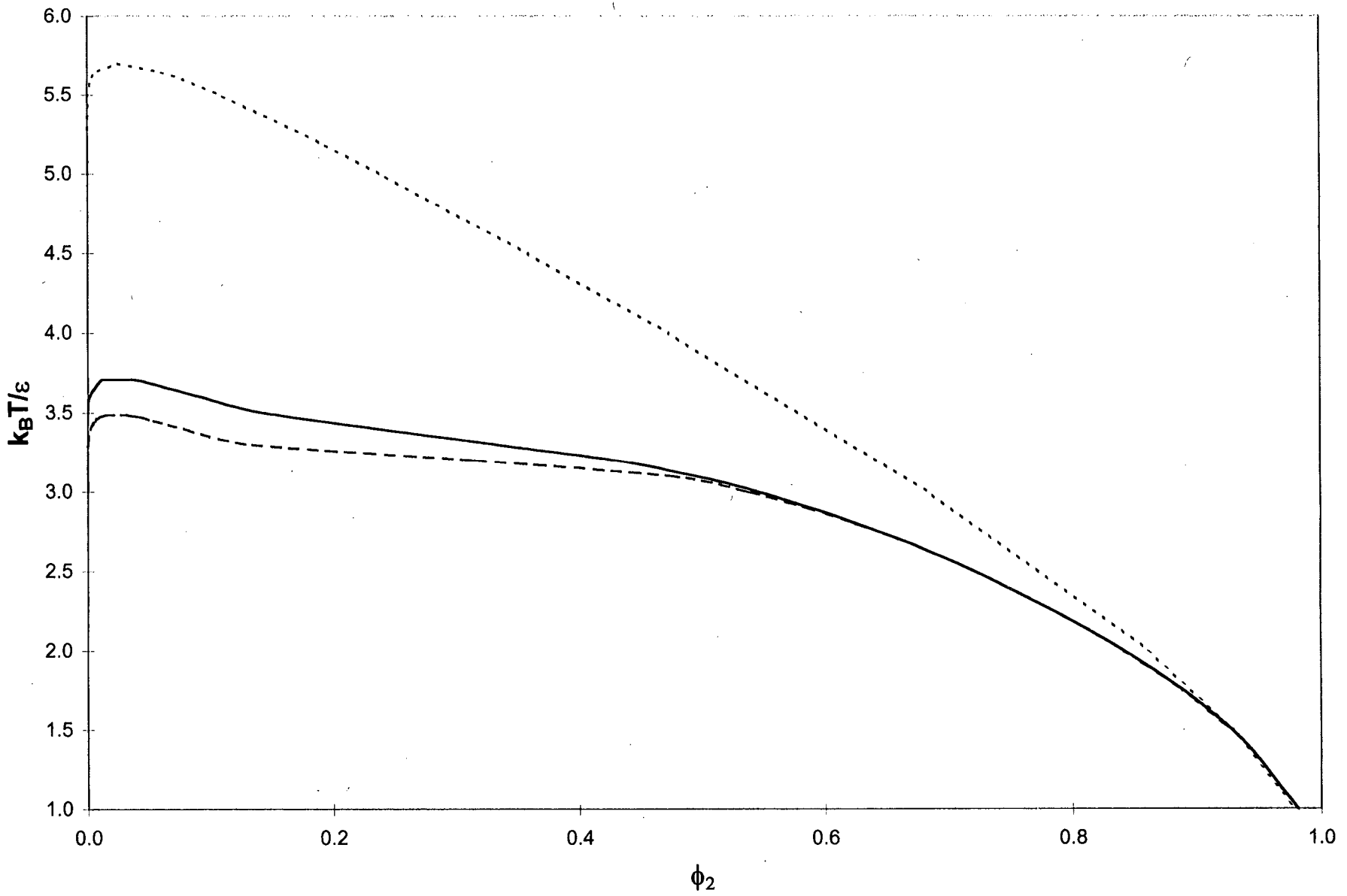
6.0
5.5
5.0
4.5
4.0
3.5
3.0
2.5
2.0
1.5
1.0
k_BT/ε
0.0
0.2
0.4
0.6
0.8
1.0
ϕ_2

Figure 14

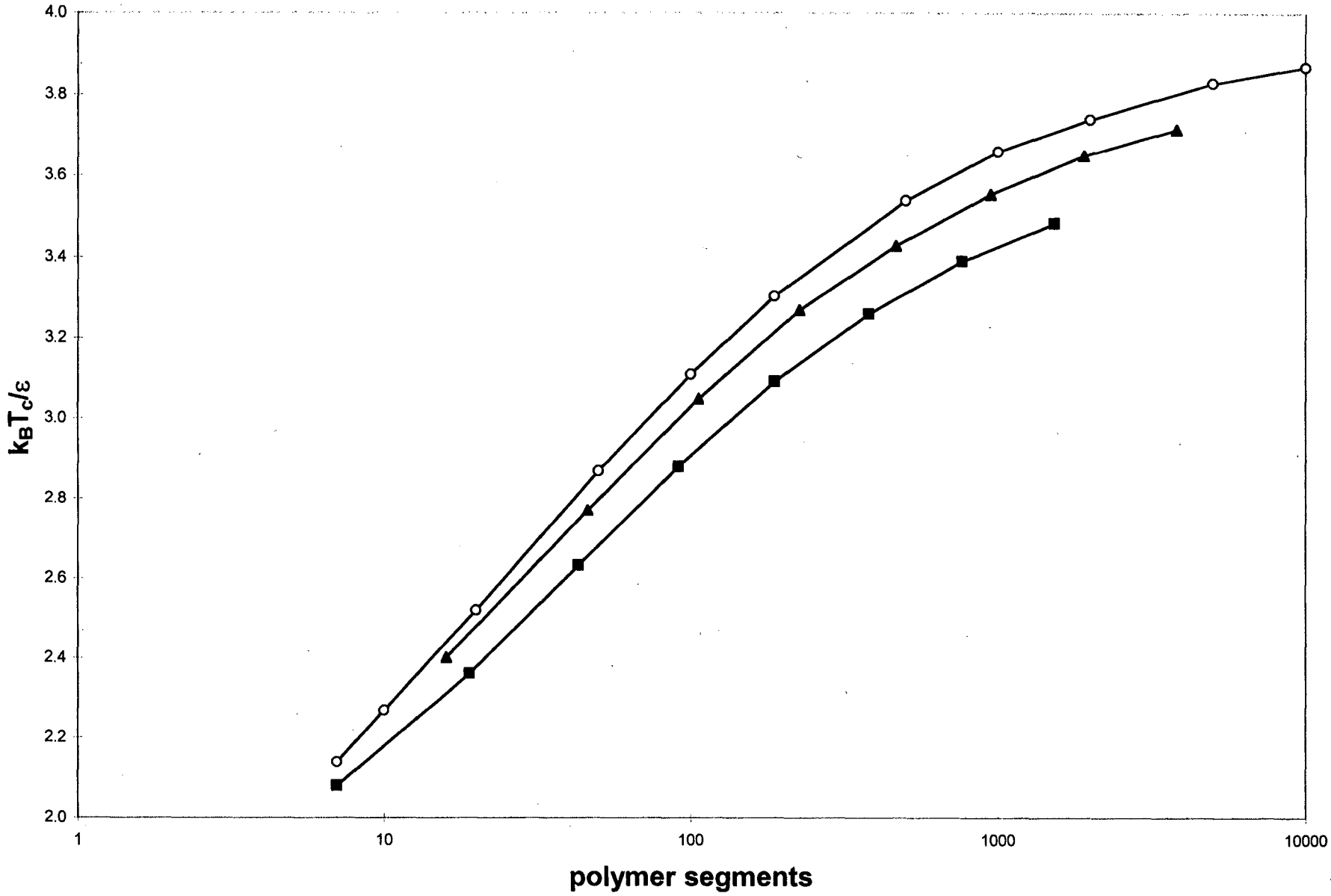
4.0
3.8
3.6
3.4
3.2
3.0
2.8
2.6
2.4
2.2
2.0
$k_B T_c/\varepsilon$
1
10
100
1000
10000
polymer segments

Figure 15

Ernest Orlando Lawrence Berkeley National Laboratory
One Cyclotron Road | Berkeley, California 94720

Prepared for the U.S. Department of Energy under Contract No. DE-AC03-76SF00098